

A stopping layer concept to improve the spatial resolution of gas-electron-multiplier neutron detector

Jianjin Zhou(周建晋), Jianrong Zhou(周健荣), Xiaojuan Zhou(周晓娟), Lin Zhu(朱林), Jianqing Yang(杨建清), Guian Yang(杨桂安), Yi Zhang(张毅), Baowei Ding(丁宝卫), Bitao Hu(胡碧涛), Zhijia Sun(孙志嘉), Limin Duan(段利敏), and Yuanbo Chen(陈元柏)

Citation: Chin. Phys. B, 2022, 31 (**5**): 050702. DOI: 10.1088/1674-1056/ac398e
Journal homepage: http://cpb.iphy.ac.cn; http://iopscience.iop.org/cpb

What follows is a list of articles you may be interested in

Finite element simulation of Love wave sensor for the detection of volatile organic gases

Yan Wang(王艳), Su-Peng Liang(梁苏鹏), Shu-Lin Shang(商树林),Yong-Bing Xiao(肖勇兵), and Yu-Xin Yuan(袁宇鑫)

Chin. Phys. B, 2022, 31 (**3**): 030701. DOI: 10.1088/1674-1056/ac3ec9

X-ray focusing using an x-ray lens composed of multi-square polycapillary slices

Kai Pan(潘凯), Tian-Cheng Yi(易天成), Zhao Wang(王曌), Mo Zhou(周末), Yu-De Li(李玉德), Zhi-Guo Liu(刘志国), Xiao-Yan Lin(林晓燕), and Tian-Xi Sun(孙天希)

Chin. Phys. B, 2022, 31 (**2**): 020701. DOI: 10.1088/1674-1056/ac381a

Effect of staggered array structure on the flow field of micro gas chromatographic column

Daohan Ge(葛道晗), Zhou Hu(胡州), Liqiang Zhang(张立强), and Shining Zhu(祝世宁)

Chin. Phys. B, 2022, 31 (**1**): 010701. DOI: 10.1088/1674-1056/ac0902

A modified analytical model of the alkali-metal atomic magnetometer employing longitudinal carrier field

Chang Chen(陈畅), Yi Zhang(张燚), Zhi-Guo Wang(汪之国), Qi-Yuan Jiang(江奇渊), Hui Luo(罗晖), and Kai-Yong Yang(杨开勇)

Chin. Phys. B, 2021, 30 (**5**): 050707. DOI: 10.1088/1674-1056/abd7d3

Miniature quad-channel spin-exchange relaxation-free magnetometer for magnetoencephalography

Jian-Jun Li(李建军), Peng-Cheng Du(杜鹏程), Ji-Qing Fu(伏吉庆), Xu-Tong Wang(王旭桐), Qing Zhou(周庆), Ru-Quan Wang(王如泉)

Chin. Phys. B, 2019, 28 (**4**): 040703. DOI: 10.1088/1674-1056/28/4/040703

A stopping layer concept to improve the spatial resolution of gas-electron-multiplier neutron detector

Jianjin Zhou(周建晋)[1,2,3,5], Jianrong Zhou(周健荣)[2,3,4,†], Xiaojuan Zhou(周晓娟)[2,3], Lin Zhu(朱林)[2,3,4], Jianqing Yang(杨建清)[2,3], Guian Yang(杨桂安)[2,3], Yi Zhang(张毅)[1], Baowei Ding(丁宝卫)[1,‡], Bitao Hu(胡碧涛)[1], Zhijia Sun(孙志嘉)[2,3,4,§], Limin Duan(段利敏)[5], and Yuanbo Chen(陈元柏)[2,3,4]

[1] *School of Nuclear Science and Technology, Lanzhou University, Lanzhou* 730000, *China*
[2] *Spallation Neutron Source Science Center, Dongguan* 523803, *China*
[3] *State Key Laboratory of Particle Detection and Electronics, Institute of High Energy Physics, Chinese Academy of Sciences, Beijing* 100049, *China*
[4] *University of Chinese Academy of Sciences, Beijing* 100049, *China*
[5] *Institute of Modern Physics, Chinese Academy of Sciences, Lanzhou* 730000, *China*

(Received 1 October 2021; revised manuscript received 11 November 2021; accepted manuscript online 15 November 2021)

In recent years, gas electron multiplier (GEM) neutron detectors have been developing towards high spatial resolution and high dynamic counting range. We propose a novel concept of an Al stopping layer to enable the detector to achieve sub-millimeter (sub-mm) spatial resolution. The neutron conversion layer is coated with the Al stopping layer to limit the emission angle of ions into the drift region. The short track projection of ions is obtained on the signal readout board, and the detector would get good spatial resolution. The spatial resolutions of the GEM neutron detector with the Al stopping layer are simulated and optimized based on Geant4GarfieldInterface. The spatial resolution of the detector is 0.76 mm and the thermal neutron detection efficiency is about 0.01% when the Al stopping layer is 3.0 μm thick, the drift region is 2 mm thick, the strip pitch is 600 μm, and the digital readout is employed. Thus, the GEM neutron detector with a simple detector structure and a fast readout mode is developed to obtain a high spatial resolution and high dynamic counting range. It could be used for the direct measurement of a high-flux neutron beam, such as Bragg transmission imaging, very small-angle scattering neutron detection and neutron beam diagnostic.

Keywords: high spatial resolution, Al stopping layer, GEM neutron detector, spallation neutron source

PACS: 07.07.Df, 29.40.Gx, 28.20.Pr, 61.05.F– **DOI:** 10.1088/1674-1056/ac398e

1. Introduction

Neutron is an important probe for research on matter and in nuclear physics. The pulsed spallation neutron sources, such as SNS in the US,[1] ISIS in the UK,[2] J-PARC in Japan[3] and CSNS in China,[4] have been established to study structures and dynamic behavior of materials. The Bragg-edge transmission imaging can reveal the crystal structure and stress distribution in materials by energy-dependent neutron transmission point-by-point over a sample.[5] The very small-angle neutron scattering can obtain information of micron-scale molecules by scattering neutron detection at very small angles on the direct beam.[6] The neutron beam diagnostic can provide different-position information of the neutron beam through the direct beam measurement.[7] These applications require a neutron detector with a sub-mm spatial resolution and high dynamic counting range. The traditional ^{3}He-based neutron detector cannot reach sub-mm spatial resolution and cannot handle counting rate above 100 kHz owing to the low drift velocity of ions.[8] Moreover, the shortage of ^{3}He and its massive use in USA have led to high price of ^{3}He gas.[9] Therefore, it is urgent to develop an alternative neutron detector.

Gas electron multiplier (GEM) detectors are widely used in high energy physics thanks to good spatial solution and timing properties, excellent counting rate, a large area coverage possibility, radiation hardness and so on.[10] GEM detectors can also detect neutral particles, such as neutrons by combining neutron conversion materials. Boron-10 is an ideal neutron converter isotope due to the advantages of large neutron capture cross-sections ($\sigma = 3843$ bar for 25 meV), easy to obtain, low cost and stable chemical properties. The traditional GEM uses FR4 or Kapton, which have high hydrogen content, as substrate. In order to reduce neutron scattering and absorption by GEM, Glass (G) GEM[11] and low-temperature co-fired ceramic (LTCC) GEM[12] have been developed in Japan, and composite ceramic GEM[13] has been developed in China. The GEM-based neutron detector using boron as neutron converter has been investigated and developed in last few decade years.[14–20] The CASCADE neutron detector was developed at Heidelberg University,[15] and has a spatial resolution of 2.6 mm at ambient gas pressure. The sealed ceramic GEM neutron detector was researched at CSNS,[20] and has a spatial

†Corresponding author. E-mail: zhoujr@ihep.ac.cn
‡Corresponding author. E-mail: dingbw@lzu.edu.cn
§Corresponding author. E-mail: sunzj@ihep.ac.cn

© 2022 Chinese Physical Society and IOP Publishing Ltd

resolution of 2.7 mm. There were some methods to improve spatial resolution. The spatial resolution of the CASCADE detector was improved from 2.6 mm to 1.3 mm by increasing the pressure of working gas from 1 bar to 3.5 bar.[15] The spatial resolution of GEM neutron detector developed by J-PARC was about 1.2 mm with strip pitch of 800 μm and drift region thickness of 1 mm.[14] However, the sub-mm spatial resolution was not achieved. In recent years, the μTPC method for finding the starting point of the ion track was proposed to achieve hundreds of microns in spatial resolution.[21,22] However, it requires complex electronic systems and algorithms, as well as a large bandwidth of data. It is not suitable for the detector with high counting rate at high-flux neutron source.

This paper proposes a novel concept of the Al stopping layer that could limit the emission angle of ions to improve spatial resolution of the GEM neutron detector. The spatial resolution and neutron detection efficiency of the detector are simulated and analyzed by the Geant4GarfieldInterface.[23] The detector could not only achieve sub-mm spatial resolution, but also have a high dynamic counting range.

2. Detector concept

The detector is a single ceramic GEM chamber equipped with a 0.1-μm-thick natural boron carbide ($^{nat}B_4C$) cathode, the schematic is given in Fig. 1(a). ^{10}B captures a thermal neutron and undergoes a prompt nuclear reaction that produces alpha (α) and ^7Li emitting in opposite directions through the following two different decay channels:

$$n + {}^{10}B \rightarrow \alpha(1.78\ \text{MeV}) + {}^{7}Li(1.01\ \text{MeV})\ (\text{BR} = 6.3\%),$$
$$n + {}^{10}B \rightarrow \alpha(1.47\ \text{MeV}) + {}^{7}Li(0.84\ \text{MeV}) + \gamma(478\ \text{keV})\ (\text{BR} = 93.7\%).$$

One of them would leave $^{nat}B_4C$ and enter the working gas, and the other would stop at the cathode. The primary electrons are generated by α or ^7Li (hereinafter referred to as ion) ionized mixture gas Ar/CO_2 (90/10). Subsequently, the electrons are avalanched in the hole of ceramic GEM. Because the ions emitted isotropically and produced long tracks in the drift region after the nuclear reaction, the larger the emission angle of the ion was and the longer the track was, the ion track length of large angle emission could reach several millimeters (the range of α with 1.47 MeV in the working gas was about 7.3 mm, calculated by SRIM[24]). There was a large deviation between the centroid of track and the true position of neutron, which leads to the poor spatial resolution of the detector.

Short ion (especially α) tracks were required to obtain good spatial resolution of the GEM neutron detector. The most direct way was to reduce the thickness of drift region. Another optimization method with the stopping layer was proposed to improve the spatial solution (shown in Fig. 1(b)). The stopping material was coated onto $^{nat}B_4C$ to restrict the emission angle of ions. The large emission angles would be reduced, and the track length of ions emitted at a small angle would be shorter in the working gas. There was short track projection of the ions on the signal readout board. The detector with the stopping layer could obtain better spatial resolution than that without. The two methods were investigated in Subsections 4.1 and 4.2, respectively. The stopping material should have a strong combination with $^{nat}B_4C$ and an extremely low neutron cross section. In addition, the material was not activated by neutron with radioactivity, which ensured that the detector had a clean background. Thus, Al was selected as the material of the stopping layer.

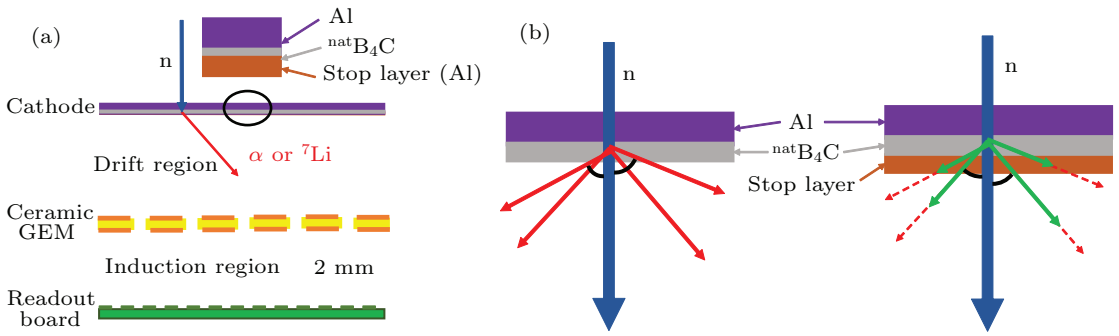


Fig. 1. (a) Schematic view of the detector concept. (b) Principal diagram of the Al stopping layer method.

3. Monte Carlo simulations

Geant4 is an open-source software toolkit to simulate the passage of particles through matter.[25] Garfield++ is a toolkit for the detailed simulation of particle detectors that use gas and semiconductors as the sensitive medium.[26] In this work, the Geant4GarfieldInterface was employed for the spatial resolution simulations of the GEM neutron detector. The simulation flow chart is shown in Fig. 2. The detector structure shown in Fig. 1(a) was constructed in the Geant4. FTFP_BERT_HP physics list, a high precision neutron model below 20 MeV in Geant4, was employed to describe ^{10}B (n, α)^7Li. Traditionally, G4PAIModel (Geant4 photo absorption ionization) is designed for the transport of fast particles in thin absorbers, but it has recently been extended to include

low energy primary particle.[27] It was used to generate the primary electrons in mixture gas, at which point Garfield++ took over. MAGBOLTZ[28] in Garfield++ was used to calculate the transport properties of electrons in mixture gas according to the detector structure and the field maps. Garfield++ provides the interfaces to HEED,[29] a PAI model similar to G4PAIModel. The HEED PAI could be used to propagate the δ-electrons from ions by using method TransportDeltaElectron() of class TrackHeed. The G4PAIModel was combined with the HEED PAI by the parameterization physics process of Geant4. It was paramount that the simulation to produce the correct number of electron–ion pairs. The lower production cut was set 20.9 eV, a value recommended in Ref. [23], which was also verified in the program.

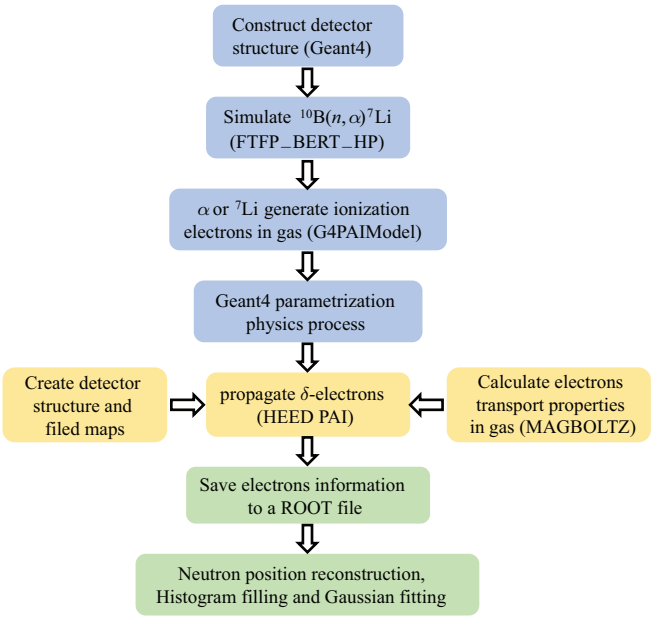


Fig. 2. The flowchart of the spatial resolution simulation based on Geant4GarfieldInterface. The blue elements represent steps taking place in Geant4, yellow elements indicate actions taking place in Garfield++ and green elements mean the steps taking place in ROOT.

Since HEED is not multithread-processor safe, only the Geant4 sequential mode can be used in combination with HEED. Because the number of electrons in drift region is around 10^4, the simulation of electron drift, diffusion, and avalanche effected by the electric field is very time-consuming. It is difficult to simulate a lot of neutron events. To evaluate the effect of electron drift, diffusion, and avalanche on the spatial resolution, the x-rays with 5.9 keV were randomly incident into the sensitive region of the ceramic GEM detector (Fig. 1(a)) in Garfield++. According to the deviation between reconstructing position and incident position of x-rays, the intrinsic spatial resolution (FWHM) of the detector was about 61 μm (shown in Fig. 3). By contrast, the ion track lengths were several millimeters in drift region. It was thus reasonable to neglect the influence of electron movement, and this process was omitted in the code. The electrons information of drift region was saved to ROOT[30] files.

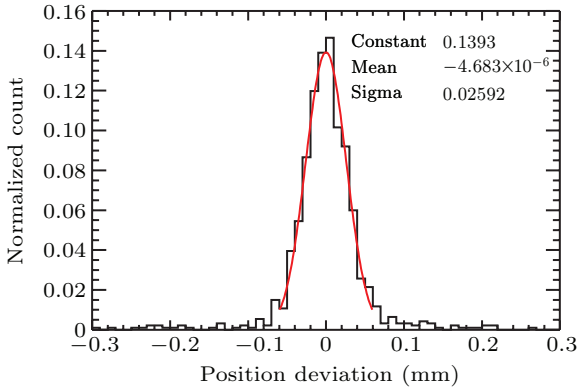


Fig. 3. The intrinsic spatial resolution of the ceramic GEM detector, about 61 μm (FWHM).

Two readout structures were obtained for the reconstruction of the neutron position: cross strip readout and pad pixel readout. If there are N channels in each of the X and Y directions, the number of electronic channels is $N+N$ for cross strip readout and that is $N\times N$ for pad pixel readout. The latter requires much more electronic channels than the former, which means that there are more costs and more complex algorithm. There are also two readout methods: analog readout and digital readout. The analog readout can obtain the detailed information about signals, thereby it can obtain better spatial resolution. However, it has more stringent requirements on electronics, involving the more complex algorithm and the higher data transmission capacity, which means that it may not work well in the high counting rate mode. By comparison, the digital readout was fast, which only registers whether the signals exceed the threshold. During neutron position reconstruction, a simple and fast readout mode was employed, the readout structure was cross strip readout, and the readout method was digital readout. Because the minimum pixel of digital readout is the pitch of strips, which affects the spatial resolution of the detector. The spatial resolutions of strips with eight pitches, ranging from 200 μm to 1600 μm (200 μm interval), were simulated and analyzed. For a neutron event, the positions of electrons generated by the ions were filled into the histograms with different bin widths. Each bin width corresponds to a strip pitch. The neutron position was calculated by $x=\frac{1}{N}\sum x_i$, where x is the reconstructed neutron position, N and x_i are the number and center coordinate of bins with nonzero counts, respectively. The spatial resolutions (FWHM) of the detector with different strip pitches were obtained by the Gaussian fitting of the reconstructed neutron events ($>10^4$) statistics.

4. Results and discussion

The spatial resolution of detector was simulated and analyzed based on Geant4GarfieldInterface. There were two methods, i.e., reducing the thickness of drift region and increasing the thickness of Al stopping layer, to reduce the track length and emission angle of ions to improve the spatial res-

olution of the GEM detector. The optimization results of the two methods were elaborated.

4.1. Optimization of drift region thickness

The track length of ions is directly related to the thickness of drift region. The narrow drift region thickness can shorten the ions track length, but it leads to the low energy deposit of ions, which cannot yield a good signal-to-noise ratio and could increase the difficulty of detector design. The spatial resolutions of different drift region thicknesses (1 mm, 2 mm, and 4 mm) were performed with different strip pitches and digital readout (shown in Fig. 4). The highest spatial resolution was obtained with 1 mm drift region, because the track length of ions was the shortest in this case. For the same drift region thickness, the spatial resolution was improved as the pitch of strip was decreased, which resulted from the fact that the smaller the pitch of strip was, the higher the accuracy of digital readout was. However, the spatial resolution tended to a stable value when the pitch of strip was less than 600 μm. There was little difference in the reconstructed neutron positions because the smaller the strip pitch was, the more the strips with signals there were for a neutron event. The best spatial resolution that the GEM neutron detector could achieve was about 1.05 mm.

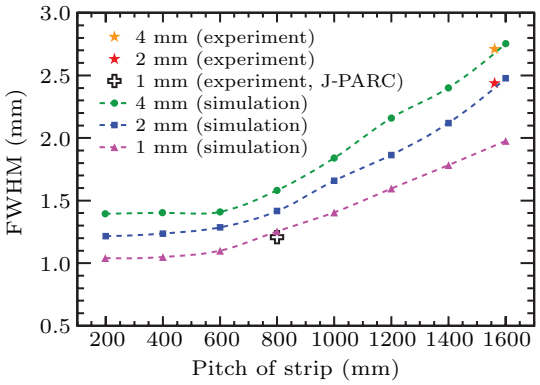


Fig. 4. The spatial resolution as a function of the strip pitch for different drift region thicknesses.

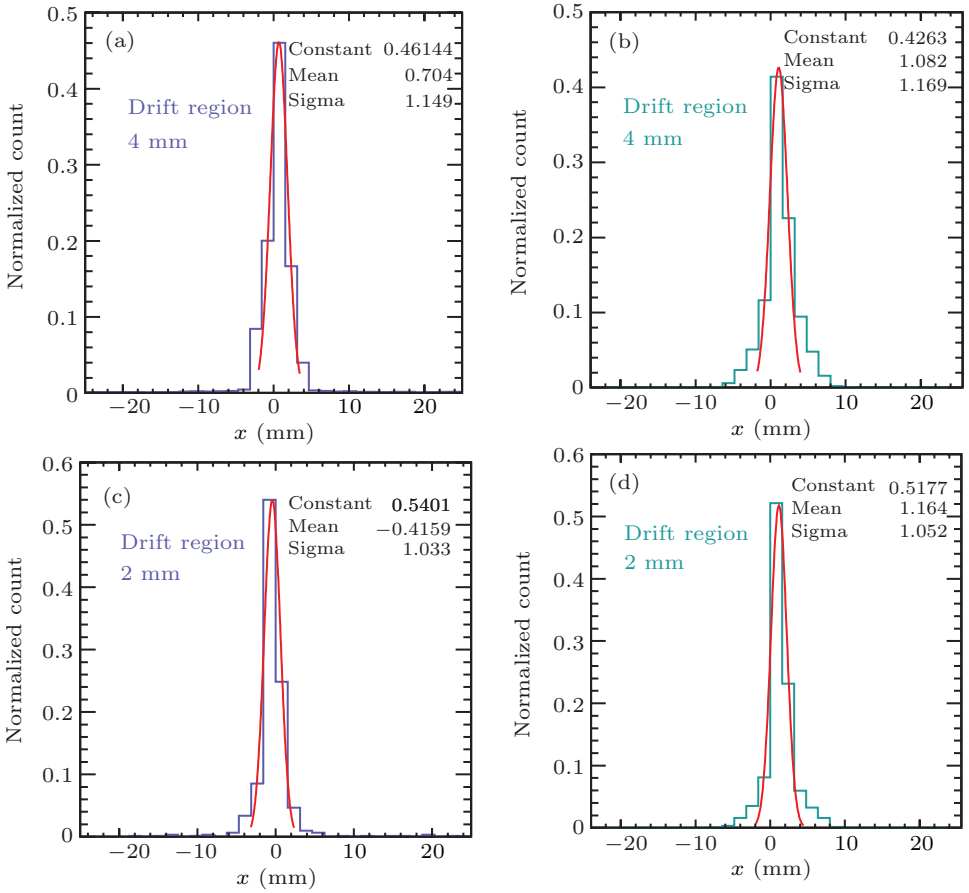


Fig. 5. The spatial resolutions of experiment and simulation with 4 mm and 2 mm drift region thickness. The experimental results with a 1563 μm strip pitch were 2.71 mm (a) and 2.43 mm (c). The simulation results with a 1600 μm strip pitch were 2.75 mm (b) and 2.48 mm (d).

The spatial resolutions of detector prototype with drift region thicknesses of 2 mm and 4 mm were measured at BL20 of CSNS. The schematic of the prototype is given in Fig. 1(a). It had a sensitive area of 50 mm × 50 mm. The cathode was a 100-μm-thick Al plate that was coated with 0.1 μm $^{nat}B_4C$. The ceramic GEM was employed for the electrons avalanche, and it was a double copper coated ceramic foil with 200 μm thickness, the holes with 200 μm diameter and 600 μm pitch were drilled and the 80 μm hole rims were etched by print circuit board technology.[13] There were 64 electronic channels ($32X + 32Y$) in total on the readout board with cross strip, where the strip pitch was 1563 μm. A 4-mm-thick cadmium

mask with a 0.27 mm hole was assembled in front of the incident window of the prototype. The spatial resolutions of the prototype with drift region thicknesses of 2 mm and 4 mm are shown in Fig. 4 (marked with stars). The detailed results of simulation and experiment are shown in Fig. 5. When the drift region was 4 mm and 2 mm thick, the spatial resolutions of the detector prototype with a 1563 μm strip were 2.71 mm (Fig. 5(a)) and 2.43 mm (Fig. 5(c)), respectively. The simulation results with a 1600 μm strip pitch were 2.75 mm (Fig. 5(b)) and 2.48 mm (Fig. 5(d)), respectively. Because the strip pitches were not consistent with one another, the simulation results were slightly larger than the experimental results, which also verified the accuracy of the simulation method. In addition, the spatial resolution of GEM neutron detector developed by J-PARC,[14] with a 1 mm drift region thickness and 800 μm strip pitch, was approximately 1.2 mm (marked with a cross in Fig. 4), which was also consistent with the simulation result.

4.2. Optimization of Al stopping layer thickness

The sub-mm spatial resolution could not be achieved only by shortening the thickness of drift region, because the emission angle of ions was large, and the most probable angle was about 83° (shown in Fig. 6(b)). The method of the Al stopping layer was investigated. The range of α with 1.47 MeV in the Al material was about 4.6 μm, given by SRIM. The spatial resolutions with the Al stopping layer thicknesses of 2.0 μm and 3.0 μm were simulated, and those of drift region thickness were 1 mm and 2 mm. The results with various strip pitches are shown in Fig. 6(a). No matter whether the Al layer was 2.0 μm or 3.0 μm thick, the spatial resolution of 1 mm drift region thickness was better than that of 2 mm drift region thickness with the same strip pitch, which was the same as that in Subsection 4.1. The spatial resolutions of the 3.0 μm Al layer for both drift region thicknesses of 1 mm and 2 mm were better than those of the 2.0 μm Al layer, because the emission angle of ions was smaller when the Al layer was thicker. When the Al layer was 2.0 μm or 3.0 μm thick, the most probable emission angles of ions were about 47° and 28°, respectively (shown in Fig. 6(b)). When the thickness of the Al layer was 3.0 μm, the spatial resolution decreased linearly as the strip pitch decreased. Because the projection of the ion track was very short, and the spatial resolution was only affected by the strip pitch. When 0.1 μm $^{nat}B_4C$ was coated with 3.0 μm Al and the strip pitch was 600 μm, the spatial resolution of the detector with 2 mm drift region was simulated as approximately 0.76 mm. The GEM neutron detector with the sub-mm spatial resolution was achieved by using the Al stopping layer and a simple and fast signal readout mode, which could be used for highly precise neutron imaging and neutron scattering.

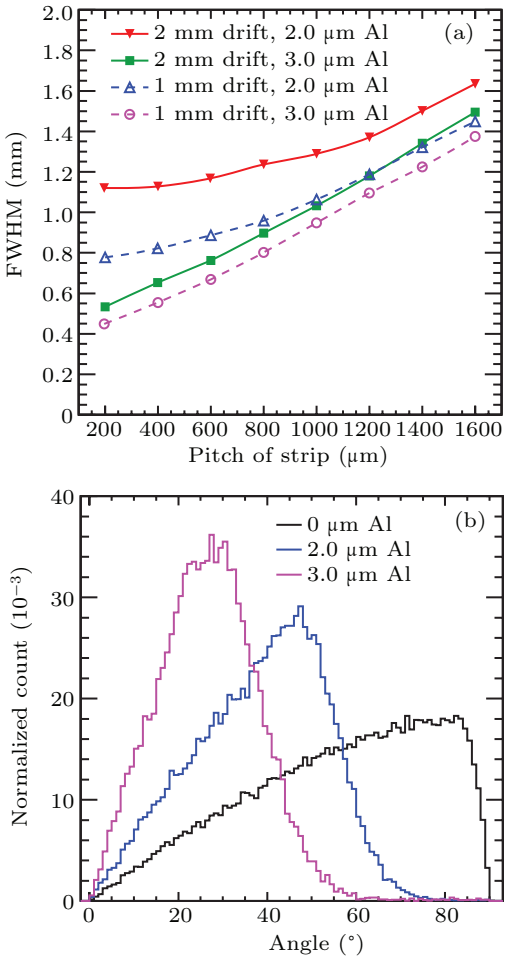


Fig. 6. (a) The spatial resolution as a function of strip pitches with drift region thicknesses (2 mm and 1 mm) and Al stopping layer thicknesses (2.0 μm and 3.0 μm). (b) The ion emission angle distribution with different thicknesses of the Al stopping layer.

4.3. Detection efficiency with neutron wavelength

The spallation neutron source has a wide neutron energy spectrum. The detection efficiencies of 0.1-μm-thick $^{nat}B_4C$ at different neutron wavelength were simulated, when the thicknesses of the Al stopping layer were 0.0 μm, 2.0 μm and 3.0 μm (shown in Fig. 7). For the thermal neutron (1.8 Å), the detection efficiency of the detector without Al layer was about 0.08%. If a lower detection efficiency is required, a thinner $^{nat}B_4C$ would be needed. However, further reducing the thickness of $^{nat}B_4C$ would lead to poor uniformity in the detector sensitive area due to the limitation of coating technology. The stopping layer was a good solution for lowering detection efficiency while ensuring the uniformity of the detector. When the thicknesses of the Al stopping layer were 2.0 μm and 3.0 μm, the detection efficiencies were about 0.02% and 0.01%, respectively. The low neutron detection efficiency of the Al stopping layer and the high counting rate of GEM enable the detector to have a very high dynamic counting range. The detector could be used for the direct measurement of the high flux neutron beam. If higher detection efficiency was required, the ^{10}B with better thickness and higher abundance could be employed as the neutron conversion layer, and the cascade method of

multi-conversion layer could also be adopted. There was a balance between the detection efficiency and the thickness of the neutron conversion layer and the stopping layer to achieve sub-mm spatial resolution.

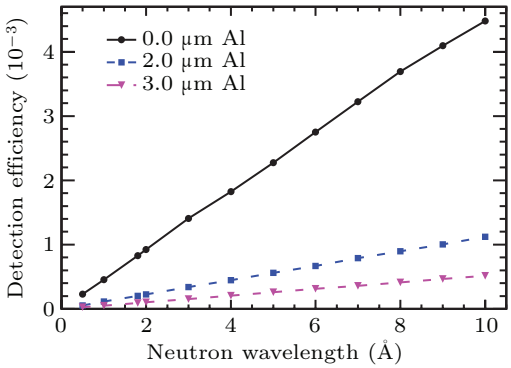


Fig. 7. The neutron detection efficiency as a function of the neutron wavelength without the Al stopping layer and with different thicknesses of the Al stopping layer.

5. Conclusion and outlook

This work examined the methods of achieving the GEM neutron detector with sub-mm spatial resolution for the high flux neutron source. A novel concept of an Al stopping layer was proposed, it could constrain the emission angle of ions to improve the spatial resolution of the detector. The detector structure was optimized based on Geant4GarfieldInterface. A simple and fast signal readout mode, i.e., cross strip and digital readout, was employed to reconstruct neutron position. The spatial resolutions of different drift region thicknesses were investigated, and some results were verified with the experimental results. The spatial resolutions of 1 mm drift region with 2.0 μm Al layer, 1 mm drift region with 3.0 μm Al layer, 2 mm drift region with 2.0 μm Al layer and 2 mm drift region with 3.0 μm Al layer were studied. When Al stopping layer was 3.0 μm thick, drift region was 2 mm thick and the strip pitch was 600 μm, a spatial resolution of 0.76 mm was achieved, and the thermal neutron detection efficiency was about 0.01%. The detector with a simple structure and a fast readout mode had sub-mm spatial resolution and high dynamic counting range, which could be used for direct measurement of the high-flux neutron beam, and could carry out Bragg transmission imaging, beam diagnosis and very small-angle scattering neutron detection. In future work, the spatial resolution of the ceramic GEM neutron detector with the Al stopping layer will be measured at CSNS. If the higher neutron detection efficiency is required, the cascaded detector structure will be developed with the optimized thickness of neutron conversion layer (concentrated ^{10}B material) and the Al stopping layer.

Acknowledgements

This work was supported by the National Key R&D Program of China (Grant No. 2017YFA0403702), the National Natural Science Foundation of China (Grant Nos. 11574123, 11775243, 12175254, and U2032166), Youth Innovation Promotion Association CAS and Guangdong Basic and Applied Basic Research Foundation (Grant No. 2019A1515110217), and the Xie Jialin Foundation, China (Grant No. E1546FU2).

References

[1] White M 2002 *AIP Conf. Proc.* **613** 15
[2] Thomason J W G 2019 *Nucl. Instrum. Methods Phys. Res. Sect. A* **917** 61
[3] Oyama Y 2006 *Nucl. Instrum. Methods Phys. Res. Sect. A* **562** 548
[4] Chen H S, Chen Y B, Wang F W, Liang T J, Jia X J, Ji Q, Hu C M, He W, Yin W, He K, Zhang B Y and Wang L S 2018 *Sci. Rep.* **29** 2
[5] Sato H, Takada O, Iwase K, Kamiyama T and Kiyanagi Y 2010 *J. Phys.: Conf. Ser.* **251** 012070
[6] Jacques D A and Trewhella J 2010 *Protein Sci.* **19** 642
[7] Croci G, Claps G, Cavenago M, Palma M D, Grosso G, Murtas F, Pasqualotto R, Cippo E P, Pietropaolo A, Rebai M, Tardocchi M, Tollin M and Gorini G 2013 *Nucl. Instrum. Methods Phys. Res. Sect. A* **720** 144
[8] Hendricks R W 1969 *Rev. Sci. Instrum.* **40** 1216
[9] Cho A 2009 *Science* **326** 778
[10] Sauli F 1997 *Nucl. Instrum. Methods Phys. Res. Sect. A* **386** 531
[11] Takahashi H, Mitsuya Y, Fujiwara T and Fushie T 2013 *Nucl. Instrum. Methods Phys. Res. Sect. A* **724** 1
[12] Takeuchi Y, Komiya K, Tamagawa T and Zhou Y 2020 *J. Phys.: Conf. Ser.* **1498** 012011
[13] Zhou J R, Zhou X J, Zhou J J, Jiang X F, Yang J Q, Zhu L, Yang W Q, Yang T, Xu H, Xia Y G, Yang G A, Xie Y G, Huang C Q and Hu B T, Sun Z J and Chen Y B 2020 *Nucl. Eng. Technol.* **52** 1277
[14] Ohshita H, Uno S, Otomo T, Koike T, Murakami T, Satoh S, Sekimoto M and Uchida T 2010 *Nucl. Instrum. Methods Phys. Res. Sect. A* **623** 126
[15] Klein M and Schmidt C J 2011 *Nucl. Instrum. Methods Phys. Res. Sect. A* **628** 9
[16] Croci G, Claps G, Caniello R, Cazzaniga C, Grosso G, Murtas F, Tardocchi M, Vassallo E, Gorini G, Horstmann C, Kampmann R, Nowak G and Stoermer M 2013 *Nucl. Instrum. Methods Phys. Res. Sect. A* **732** 217
[17] Köhli M, Allmendinger F, Häußler W, Schröder T, Klein M, Meven M and Schmidt U 2016 *Nucl. Instrum. Methods Phys. Res. Sect. A* **828** 242
[18] Zhou J R, Zhou X J, Zhou J J, Teng H Y, Yang J Q, Ma Y C, Zhou K, Xia Y G, Xiu Q L, Yang T, Jiang X F, Zhu L, Yang W Q, Yang G A, Xie Y G, Hu B T, Sun Z J and Chen Y B 2020 *Nucl. Instrum. Methods Phys. Res. Sect. A* **962** 163593
[19] Zhou J R, Xiu Q L, Zhou X J, Zhou J J, Ma L L, Schmidt C J, Klein M, Xia Y G, Zhu L, Huang C Q, Sun G G, Hu B T, Sun Z J and Chen Y B 2020 *Nucl. Instrum. Methods Phys. Res. Sect. A* **953** 163051
[20] Zhou J J, Zhou J R, Zhou X J, Zhu L, Wei Y D, Xu H, Guan B J, Wu H Y, Wei K, Yang J Q, Wu X G, Yang G A, Xie Y G, Zhang Y, Wang X H, Ding B W, Hu B T, Sun Z J, Duan L M and Chen Y B 2021 *Nucl. Instrum. Methods Phys. Res. Sect. A* **995** 165129
[21] Pfeiffer D, Resnati F, Birch J, Wilton R H, Höglund C, Hultman L, Iakovidis G, Oliveri E, Oksanen E, Ropelewski L and Thuiner P 2015 *J. Instrum.* **10** P04004
[22] He Z, He S, Wu H, Xu R, Hu B, Zhang Y and Yang H 2021 *J. Instrum.* **16** P08020
[23] Pfeiffer D, Keukeleere L D, Azevedo C, Belloni F, Biagi S, Grichine V, Hayen L,. Hanu A R, Hřivnáčová I, Ivanchenko V, Krylov V, Schindler H and Veenhof R 2019 *Nucl. Instrum. Methods Phys. Res. Sect. A* **935** 121
[24] Ziegler J F, Ziegler M D and Biersack J P 2010 *Nucl. Instrum. Methods Phys. Res. Sect. A* **268** 1818
[25] Agostinelli S, Allison J, Amako K *et al.* 2003 *Nucl. Instrum. Methods Phys. Res. Sect. A* **506** 250
[26] Schindler H and Veenhof R 2018 *Garfield++*
[27] Vladimir I, John A, Alexander B *et al.* 2011 *Prog. Nucl. Sci. Technol.* **2** 898
[28] Biagi S F 1999 *Nucl. Instrum. Methods Phys. Res. Sect. A* **421** 234
[29] Smirnov I B 2005 *Nucl. Instrum. Methods Phys. Res. Sect. A* **554** 474
[30] Brun R and Rademakers F 1997 *Nucl. Instrum. Methods Phys. Res. Sect. A* **389** 81